Cell Reports

Rhythmic Food Intake Drives Rhythmic Gene Expression More Potently than the Hepatic Circadian Clock in Mice

Graphical Abstract

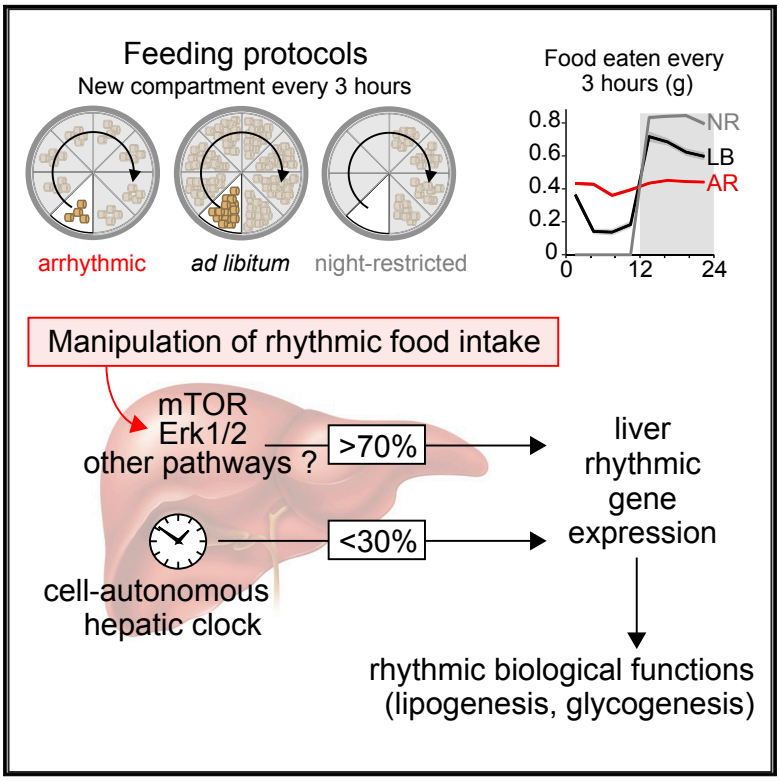

Highlights

- Manipulation of the food-intake rhythm does not impair core clock gene oscillations
- The rhythm of food intake is necessary for rhythmic expression of many liver genes
- Rhythmic food intake contributes to the rhythmic activity of mTOR and Erk1 and Erk2 pathways
- Rhythmic food intake regulates the expression of lipogenic and glycogenic enzymes

Authors

Ben J. Greenwell, Alexandra J. Trott, Joshua R. Beytebiere, ..., Patrick Finegan, Christopher Hernandez, Jerome S. Menet

Correspondence

menet@bio.tamu.edu

In Brief

A large fraction of the genome is rhythmically expressed in healthy organisms in a tissue-specific manner. Greenwell et al. report that the daily rhythm of food intake significantly contributes to rhythmic gene expression in the mouse liver without altering core clock gene oscillations.

Greenwell et al., 2019, Cell Reports 27, 649–657
April 16, 2019
https://doi.org/10.1016/j.celrep.2019.03.064

CellPress

Cell Reports
Report

Rhythmic Food Intake Drives Rhythmic Gene Expression More Potently than the Hepatic Circadian Clock in Mice

Ben J. Greenwell,[1,2] Alexandra J. Trott,[1,2] Joshua R. Beytebiere,[2] Shanny Pao,[2] Alexander Bosley,[2] Erin Beach,[2] Patrick Finegan,[2] Christopher Hernandez,[2] and Jerome S. Menet[1,2,3,*]
[1]Program of Genetics, Texas A&M University, College Station, TX 77843, USA
[2]Department of Biology, Texas A&M University, College Station, TX 77843, USA
[3]Lead Contact
*Correspondence: menet@bio.tamu.edu
https://doi.org/10.1016/j.celrep.2019.03.064

SUMMARY

Every mammalian tissue exhibits daily rhythms in gene expression to control the activation of tissue-specific processes at the most appropriate time of the day. Much of this rhythmic expression is thought to be driven cell autonomously by molecular circadian clocks present throughout the body. By manipulating the daily rhythm of food intake in the mouse, we here show that more than 70% of the cycling mouse liver transcriptome loses rhythmicity under arrhythmic feeding. Remarkably, core clock genes are not among the 70% of genes losing rhythmic expression, and their expression continues to exhibit normal oscillations in arrhythmically fed mice. Manipulation of rhythmic food intake also alters the timing of key signaling and metabolic pathways without altering the hepatic clock oscillations. Our findings thus demonstrate that systemic signals driven by rhythmic food intake significantly contribute to driving rhythms in liver gene expression and metabolic functions independently of the cell-autonomous hepatic clock.

INTRODUCTION

Nearly every mammalian cell harbors a molecular circadian clock that drives rhythmic gene expression to coordinate daily cycles in metabolism, physiology, and behavior. These clocks are synchronized to the daily environmental variation by the master circadian pacemaker located in the suprachiasmatic nucleus (SCN) of the hypothalamus, which is itself entrained to the light:dark cycle via direct retinal innervation (Bass and Takahashi, 2010; Mohawk et al., 2012). The SCN utilizes multiple cues to synchronize peripheral clocks, including rhythms in neuronal signaling, hormone secretion, body temperature, and food intake (Mohawk et al., 2012). The hierarchical organization of the circadian system positions the SCN as the master coordinator of all peripheral clocks, ensuring that they are all properly entrained to the environment and synchronized throughout the body. Entrained peripheral clocks are thought to then regulate rhythmic gene expression in a cell-autonomous manner to initiate tissue-specific circadian transcriptional programs that control the rhythmicity of biological processes (Kornmann et al., 2007; Lamia et al., 2008; Zhang et al., 2014). Experiments using temporal-restricted feeding paradigms demonstrated that the daily rhythm of food intake is a major synchronizing cue for the circadian clock and circadian transcriptional programs in the liver and other peripheral tissues (Chaix et al., 2014; Damiola et al., 2000; Hatori et al., 2012; Kawamoto et al., 2006; Saini et al., 2013; Satoh et al., 2006; Stokkan et al., 2001; Vollmers et al., 2009). However, recent evidence suggests that SCN-driven cues, in particular the rhythm of food intake, can also drive rhythmic gene expression in peripheral tissues without involving cell-autonomous molecular clocks (Atger et al., 2015; Izumo et al., 2014; Mange et al., 2017; van der Veen et al., 2006; Vollmers et al., 2009). In this study, we investigated this possibility by analyzing the role of the daily rhythm of food intake in driving circadian hepatic functions in the mouse. We found that contrary to current models, rhythmic food intake (RFI) drives the majority of rhythmic gene expression independently of the cell-autonomous hepatic clock.

RESULTS AND DISCUSSION

To characterize the contribution of RFI to circadian biology and rhythmic gene expression, we developed a feeding system that allows for the long-term manipulation of RFI in the mouse (Figure 1A). This system exposes each mouse to a new feeding compartment every 3 h. We fed mice under 3 feeding paradigms: $1/8^{th}$ of the daily food intake every 3 h (arrhythmic [AR] feeding), only at night (i.e., night-restricted [NR] feeding), or *ad libitum* (LB) (Figures 1A, S1A, and S1B). As previously shown, mice fed LB in a 12:12 h light:dark (LD12:12) cycle exhibit robust rhythms of food intake and eat 75% of their daily food intake at night (Figures 1B, 1C, and S1B). Change to the NR or AR paradigms profoundly affects the daily profile of RFI. While all mice still eat the majority of their food at night, the amount of chow eaten during the light phase varied considerably from 48.9% in AR-fed mice to 0% in NR-fed mice (and 23.8% in LB-fed mice; Figures 1B and 1C). Because AR-fed mice displayed difficulties in adapting fully to the AR-feeding paradigm and ate less from Zeitgeber time (ZT)6 to ZT12, we doubled the number of mice and separated them after 5 weeks into an AR group (robust dampening

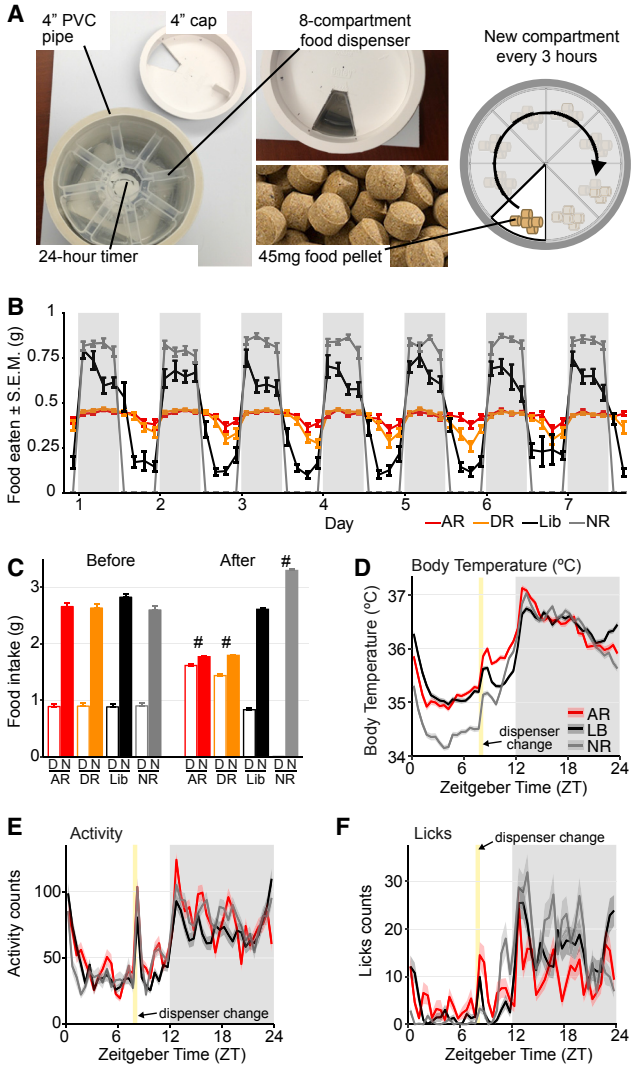

Figure 1. Mice Fed AR Remain Behaviorally Rhythmic

(A) Overview of the feeding system. An 8-compartment food dispenser is placed on a 24-h timer and capped by a lid such that only one compartment is accessible at a time.

(B) Average food eaten from each of the eight compartments for 7 consecutive days in mice acclimated to their feeding paradigm for 4 weeks (mean ± SEM; n = 18 per paradigm). AR, arrhythmic feeding (red); DR, dampened feeding rhythm (orange); LB, *ad libitum* feeding (black); NR, night-restricted feeding (gray).

(C) Quantification of the food eaten during the day and night (mean ± SEM; n = 18 per paradigm. # indicates a significant difference in food eaten during the day versus the night before and after adaptation to feeding paradigms (p value < 0.05, repeated-measures two-way ANOVA).

(D–F) Rhythms of body temperature (D), physical activity (E), and lick counts (drinking behavior) (F) for 7 consecutive days (n = 7–8 per feeding paradigm). The yellow bar indicates time of dispenser change-out at ZT8. Shading represents the SEM.

of RFI) and dampened rhythm (DR) feeding group (less robust dampening of RFI) (Figures 1B and 1C).

To determine if RFI manipulation alters other physiological and behavioral rhythms, we implanted mice with telemeters and tracked the body temperature, physical activity, and number of water bottle licks (interpreted as drinking behavior) (Figures 1D–1F and S1C–S1E). Body temperature continued to exhibit normal daily oscillations in AR and LB mice and was significantly decreased by ~1°C during the day in NR mice, potentially due to the lack of feeding during the rest phase, as shown in other studies (Damiola et al., 2000; Satoh et al., 2006) (Figures 1D and S1C). Physical activity and drinking behavior were not affected by changes in RFI and continued to exhibit robust oscillations across the 24-h day (Figures 1E, 1F, S1D, and S1E). Thus, mice fed AR remain behaviorally rhythmic and still exhibit a rhythmic drive to feed when active at night, indicating that we uncoupled the rhythm of food intake from other rhythmic behaviors in AR-fed mice.

RFI is a potent cue for synchronizing circadian rhythms in peripheral tissues (Damiola et al., 2000; Izumo et al., 2014; Kornmann et al., 2007; Saini et al., 2013; Vollmers et al., 2009). To determine if manipulation of RFI alters the rhythmic hepatic transcriptome, we collected the livers of mice fed for 5 weeks under the three different feeding paradigms in LD12:12 every 4 h for 24 h and sequenced 3′ mRNA (n = 3 per paradigm and time point). Genome-wide analysis of rhythmic gene expression, performed using four independent statistical programs (see STAR Methods for details), revealed that the number of rhythmically expressed genes under each feeding paradigm correlates with the amplitude of RFI (Figure 2A; Table S1). However, rhythmically expressed genes exhibit a relatively poor overlap between each feeding paradigm, with ~1,600 and 500 genes found to be uniquely rhythmically expressed under NR and AR feeding, respectively (Figure 2B).

To characterize the contribution of RFI to the regulation of rhythmic gene expression in the mouse liver, we focused our analysis on the three major feeding paradigms (NR, LB, and AR; see STAR Methods for details). Genes were categorized into several groups: genes rhythmic in all three feeding paradigms (named RRR for rhythmic in NR, LB, and AR), genes whose decreased rhythmicity in gene expression parallels the decreased amplitude in RFI (genes rhythmically expressed in NR and LB, but not in AR, as well as genes rhythmic in NR only, named respectively RRA and RAA), and genes that are rhythmic in AR-fed mice only (named AAR). Genes rhythmic under all three feeding paradigms (RRR genes) maintained a similar phase of expression and only exhibited a small decrease in amplitude, suggesting that RFI does not contribute much to their transcription (Figures 2C and S2A–S2C). In contrast, genes in the RRA and RAA categories, which represent a large fraction of the expressed mouse liver transcriptome (n = 2,229 genes), showed a significant dampening in gene expression with a robust decrease in amplitude that parallels the decrease in RFI oscillation (Figures 2C and S2C). Phase analysis revealed that rhythmically expressed RRR, RRA, and RAA genes maintained a well-correlated phase of expression across the 24-h day, yet most rhythmic genes were consistently phase-advanced by 1–2 h in NR- and AR-fed mice when compared to LB-fed mice (Figures S2A and S2B). Genes in the AAR category displayed an increased rhythmicity and amplitude in gene expression that is inversely correlated with the amplitude of RFI oscillation. Many of the AAR genes peak at a uniform phase at the end of

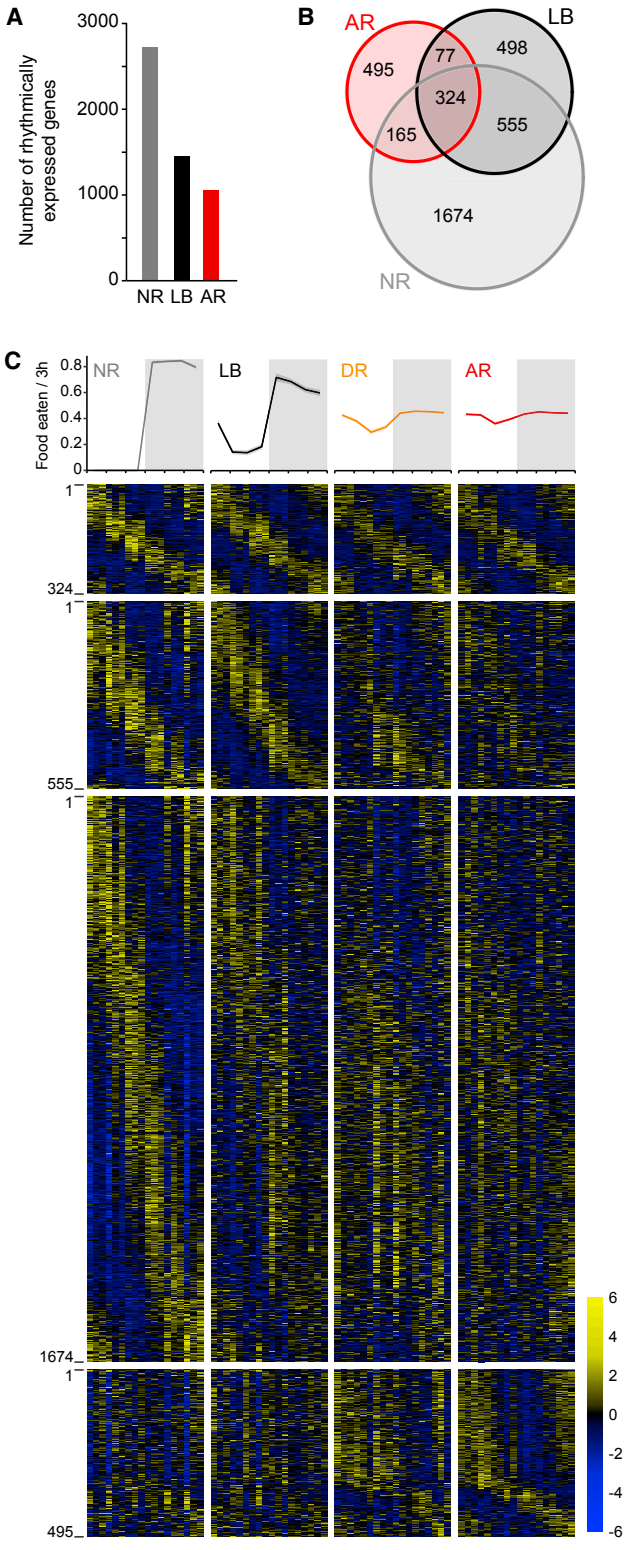

Figure 2. Manipulation of RFI Impairs Rhythmic Gene Expression in the Mouse Liver

(A) Number of rhythmically expressed genes in the liver of mice fed AR (red), LB (black), or only at night (NR; gray). See STAR Methods for details about the statistical analysis.

(B) Overlap of rhythmically expressed genes among the three feeding paradigms.

(C) Top: averaged food eaten profile. Shading represents the SEM. Bottom: heatmap of standardized expression for four categories: RRR (genes rhythmic in NR-, LB-, and AR-fed mice; 324 genes), RRA (genes rhythmic in NR- and LB-fed mice and arrhythmic in AR-fed mice; 555 genes), RAA (genes rhythmic in NR-fed mice only; 1,674 genes), and AAR (genes rhythmic in AR-fed mice only; 495 genes). Data for each column are grouped by time point (n = 3 per time point) and plotted from left to right by increasing time point starting at ZT2. Rows are sorted according to the peak phase in LB (RRR and RRA), NR (RAA), or AR (AAR). Expression and averaged feeding data for the DR mice (dampened-rhythm of food intake; orange) are shown for comparison but were not considered for analysis.

the night and/or beginning of the day in AR-fed mice, potentially indicating activation by a single pathway and/or transcription factor (Figure S2D). Pathway enrichment analysis indicates that AAR genes are involved in xenobiotic metabolism, response to infection, and protein processing in the endoplasmic reticulum (Figure S2E). While the mechanisms underlying their rhythmic expression are unclear, we suspect that most AAR genes exhibit a peak of expression at the end of the night and/or beginning of the day in AR-fed mice in response to insufficient food intake at night compared to the physiological drive to feed. Taken together, these data indicate that the amplitude of RFI significantly contributes to the genome-wide oscillation in gene expression and that more than 70% of the cycling hepatic transcriptome under LB feeding lose rhythmicity in mice fed AR.

Rhythmic gene expression in the mouse liver is thought to be mostly driven by the hepatic circadian clock in a cell-autonomous manner (Kornmann et al., 2007; Lamia et al., 2008; Vollmers et al., 2009). To determine if the hepatic molecular clock is responsible for the RFI-dependent decrease in rhythmic gene expression, we examined the expression of core clock genes. We found that all core clock genes were in the RRR category (Figures 3A and S3A; Table S2), thus suggesting that the core molecular clock in the liver is not affected by RFI manipulation and that it does not significantly contribute to the RFI-mediated changes in RRA and RAA gene expression.

Based on these results, we hypothesized that the rhythmic expression of RRA and RAA genes is mostly driven by RFI, and that the 324 RRR genes are the only genes predominantly regulated by the hepatic clock. To test this hypothesis, we determined if clock-deficient mice fed only at night could maintain the rhythmic expression of RRA and RAA genes, but not RRR genes. To this end, we analyzed a public mouse liver RNA sequencing (RNA-seq) dataset in which wild-type and *Bmal1*$^{-/-}$ mice were fed only at night (Atger et al., 2015). Visualization of gene expression revealed that most RRR genes lose rhythmicity in *Bmal1*$^{-/-}$ mice, confirming that RRR genes rely on a functional clock for rhythmic expression (Figure 3B). Interestingly, RRR genes peaking at the end of the night and/or beginning of the day in wild-type mice become constitutively expressed at high levels in *Bmal1*$^{-/-}$ mice, whereas those peaking at the end of the day/beginning of the night become constitutively expressed at low levels (Figures 3B and S3B). These results are consistent with direct transcriptional control by CLOCK:BMAL1, which binds DNA more potently in the middle of the day and whose direct target genes exhibit a similar pattern of expression in

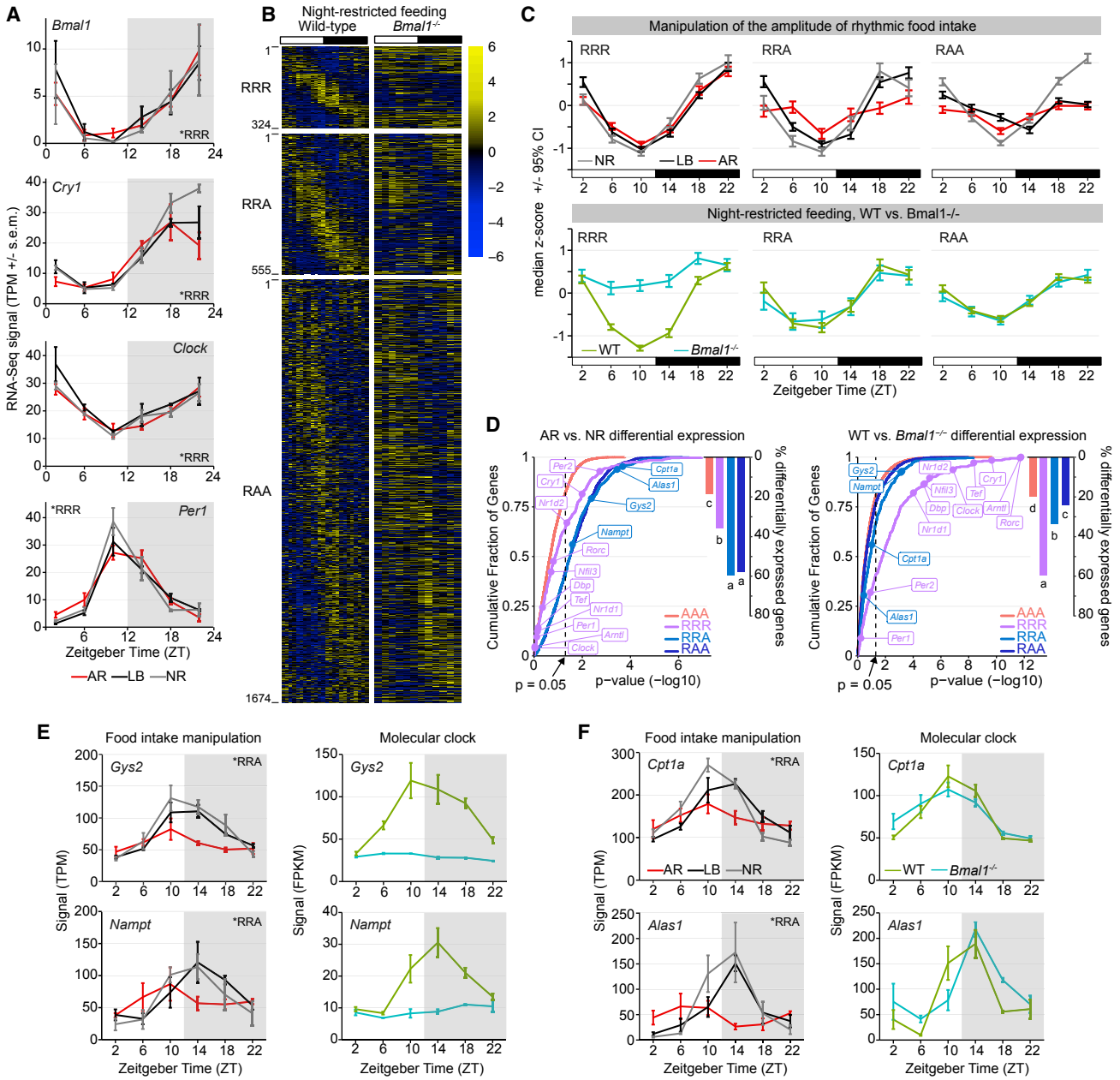

Figure 3. RFI Drives Most Hepatic Rhythmic Gene Expression Independently of the Hepatic Clock

(A) Expression of the core clock genes *Bmal1*, *Clock*, *Cry1*, and *Per1* in the liver of mice fed AR (red), LB (black), and only at night (NR; gray) (mean ± SEM; n = 3 per time point).

(B) Standardized mouse liver gene expression for wild-type and *Bmal1*$^{-/-}$ mice fed only at night, derived from a public dataset (Atger et al., 2015). The RRR, RRA, and RRA categories are represented as in Figure 2C with the same number and ordering of genes (n = 4 per time point for wild-type mice, n = 2 per time point for *Bmal1*$^{-/-}$ mice).

(C) Quantification of the median standardized expression for the RRR, RRA, and RAA categories at each time point, binned by 4-h windows of phase and shown for the ZT20–ZT24 bin. Error bars represent the 95% confidence interval. A figure including bins covering the 24-h day is provided as Figure S3B.

(D) Cumulative distributions of log-transformed p values for differential rhythmicity in gene expression between AR and NR feeding paradigms (left) and between WT and *Bmal1*$^{-/-}$ backgrounds. p values were obtained from the HANOVA (ANOVA applied on harmonic regression) metric of DODR analysis (Thaben and Westermark, 2016). The category AAA (arrhythmic gene expression in NR-, LB-, and AR-fed mice) is shown as background. The percentage of differentially rhythmic genes is displayed for each category to the right. Groups with different letters are significantly different ($p < 0.05$; Kolmogorov-Smirnov test).

(E and F) Gene expression (mean ± SEM; n = 3 per timepoint) of four *Bmal1* target genes rhythmically expressed in LB conditions yet showing differences in rhythmic expression in response to both feeding and clock function (E) or changes in feeding only (F).

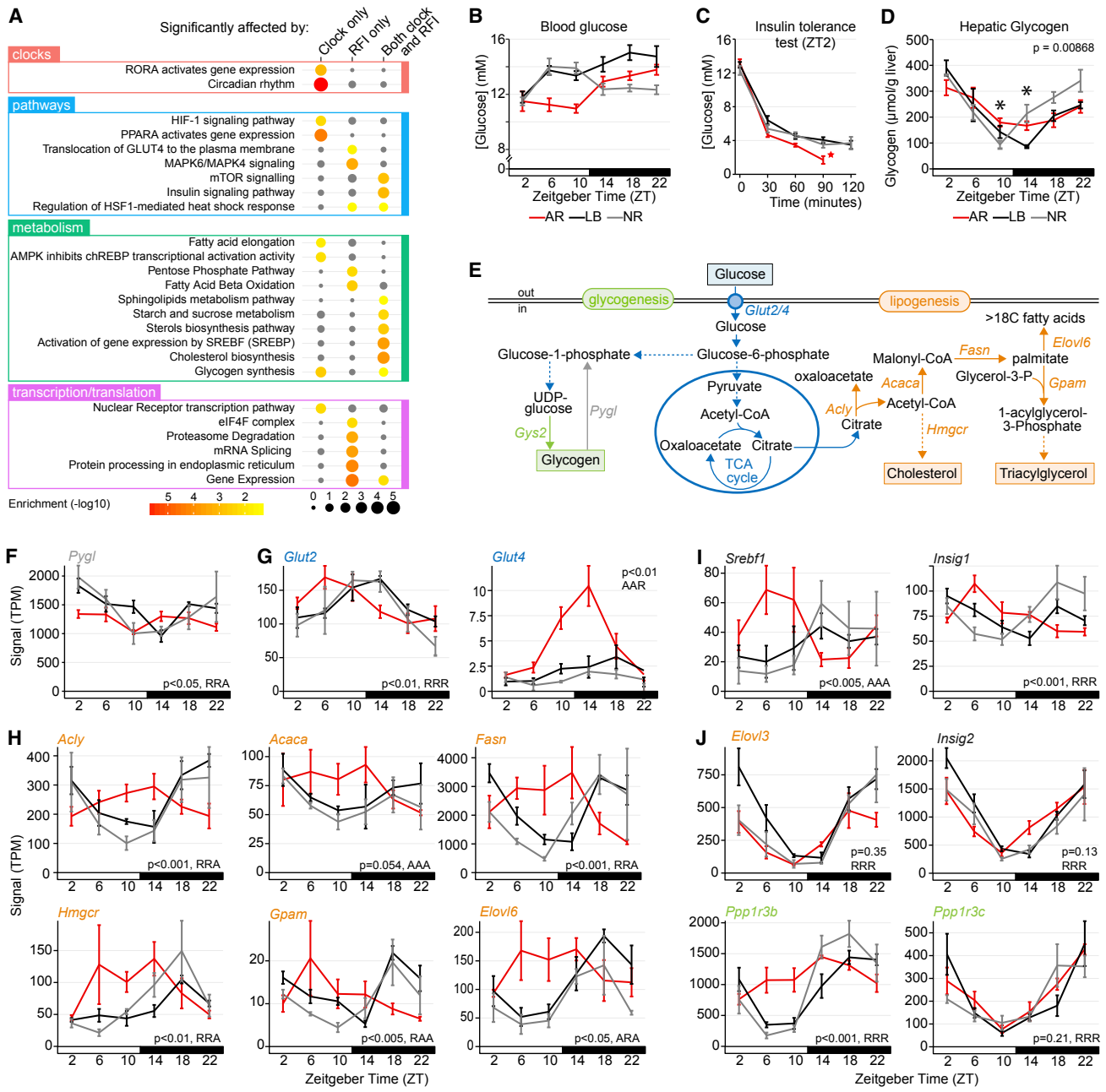

(legend on next page)

Bmal1$^{-/-}$ mice (Trott and Menet, 2018). On the other hand, visualization of RRA and RAA genes in the liver of *Bmal1*$^{-/-}$ mice fed only at night revealed that most of these genes are expressed rhythmically, indicating that their rhythmic expression is driven by RFI and not by the hepatic clock (Figures 3B and 3C). Quantification of standardized gene expression binned by phase confirmed these results; RRR genes exhibit strong effects in median gene expression in response to *Bmal1* knockout, but not to changes in RFI amplitude, whereas, conversely, RAA genes (and to a lesser extent RRA genes) show little to no response in *Bmal1*$^{-/-}$ mice but exhibit strong effects under manipulation of RFI (Figures 3C and S3B).

To further unveil the relative contribution of the hepatic clock versus RFI in initiating rhythmic gene expression in the mouse liver, we performed a statistical analysis of differential rhythmicity using the detection of differential rhythmicity (DODR) program (Thaben and Westermark, 2016). Comparison of rhythmic expression between NR-fed and AR-fed mice revealed that most genes in the RRA and RAA categories are affected by RFI manipulation and that the RRR genes were less affected (Figure 3D). However, the effects of RFI on RRR genes were significantly higher than background (calculated using genes arrhythmically expressed in all three feeding paradigms [AAA]), indicating that rhythmic expression of clock-controlled genes is still partially affected by RFI. Analysis of differential rhythmicity between wild-type and Bmal1$^{-/-}$ mice fed only at night also confirmed that genes in the RRR category were more affected by the disruption of molecular clock than genes in the RRA and RAA categories, which are at a level very close to that of the background and barely affected by Bmal1 knockout. Interestingly, genes whose rhythmic expression is preferentially regulated by RFI rather than by the clock (DODR NR- versus AR-fed mice, $p \leq 0.05$; DODR wild-type versus Bmal1$^{-/-}$ mice, $p > 0.05$) exhibit a phase distribution in NR-fed Bmal1$^{-/-}$ mice that is well correlated with the phase distribution in NR-fed wild-type mice yet globally phase-advanced by 1–2 h (Figure S3C). This suggests that feeding time alone can set the phase distribution of a large fraction of the cycling transcriptome in a clock-deficient mouse similarly to the phase distribution observed in a wild-type mouse and that the circadian clock delays the RFI-driven distribution of rhythmic gene expression by 1–2 h. Taken together, our data demonstrate that the rhythmicity of most genes in the mouse liver is predominantly driven by the rhythm of food intake and that the rhythmicity of only a few hundred genes is directly controlled by the cell-autonomous hepatic clock.

Results from the analyses of differential rhythmicity prompted us to identify rhythmic genes regulated by RFI, the hepatic clock, or both. As expected, almost all core clock genes were affected by Bmal1 knockout, but not by RFI manipulation, confirming that the molecular clock oscillations are resilient to changes in RFI amplitude (Figures 3D and S3A). However, this was not the case for Per1 and Per2, which are the entry point for the entrainment of mammalian circadian clocks (Albrecht et al., 2001; Maywood et al., 1999; Shearman et al., 1997). Per1 rhythmic expression was not affected by the molecular clock disruption or RFI manipulation and continued to oscillate normally in both NR-fed Bmal1$^{-/-}$ mice and AR-fed wild-type mice (Figures 3A and S3A). Per2 rhythmic expression was only affected by RFI manipulation, with decreased amplitude and a phase advance of 2.8 h from LB (Figure S3A), which is consistent with reports showing that Per2 expression is driven by systemic signals and not by the hepatic clock (Kornmann et al., 2007). In addition, examination of four known BMAL1 target genes encoding rate-limiting enzymes showed that their rhythmic expression in the liver, which is assumed to driven by the hepatic clock, relies on RFI (Doi et al., 2010; Hatanaka et al., 2010; Kaasik and Lee, 2004; Ramsey et al., 2009) (Figures 3E and 3F). Interestingly, the rhythmic expression of Gys2 and Nampt is also impaired in NR-fed Bmal1$^{-/-}$ mice, indicating that their rhythmic expression is controlled by both the hepatic clock and RFI (Figure 3E). However, Cpt1a and Alas1 continue to cycle with similar phases and amplitudes in NR-fed Bmal1$^{-/-}$ mice, suggesting that their rhythmic expression is driven by RFI and not the hepatic clock despite being CLOCK:BMAL1 target genes (Figure 3F).

The cell-autonomous hepatic clock is thought to drive rhythmic gene expression to temporally separate incompatible biochemical and metabolic processes (Panda, 2016). Our findings that the rhythmic expression of several rate-limiting enzymes, which were thought to be directly regulated by the hepatic clock, actually relies on the rhythm of food intake prompted us to examine at the genome-wide level the genes and pathways that are regulated by RFI, the hepatic clock, or both. Remarkably, many metabolic pathways known to be rhythmic in the mouse liver were found to be regulated by RFI (Abbondante et al., 2016; Eckel-Mahan et al., 2012) (Figure 4A;

Figure 4. RFI Contributes to the Timing of Metabolic and Signaling Pathways Independently of the Hepatic Clock

(A) Pathway enrichment for the RRR, RRA, and RAA genes (see Figure 2C) based on whether their rhythmic expression is significantly affected by *Bmal1* knockout, RFI manipulation, or both.

(B) Blood glucose levels at 6 time points (n = 12 mice per feeding paradigm; mean ± SEM).

(C) Blood glucose levels before injection of insulin (t = 0) and every 30 min after injection (mean ± SEM; n = 12 per feeding paradigm). 10 out of the 12 AR-fed mice were catatonic at t = 90 and rescued with an injection of 20% glucose (see STAR Methods).

(D) Hepatic glycogen levels (n = 3 per feeding paradigm and time point; mean ± SEM; two-way ANOVA interaction p value). The asterisks indicate $p < 0.05$ (one-way ANOVA).

(E) Schematic of the glycogenesis and lipogenesis pathways in mammals. Rate-limiting enzymes and key genes are displayed.

(F–J) Liver mRNA expression (mean ± SEM; n = 3 per timepoint) in AR-, LB-, and NR-fed mice for glycogen phosphorylase *Pygl* (F), the glucose transporters *Glut2* and *Glut4* (G), the rate-limiting enzymes for lipogenesis and cholesterol biosynthesis (H), the lipogenic transcription factor *Srebf1* and its co-regulator, *Insig1* (I), and paralog genes involved in glycogenesis and lipogenesis but showing a different response to RFI manipulation (J). For each gene, the DODR p value for AR versus NR analysis and the rhythmic category are shown.

(K) Protein expression in the liver of AR-, LB-, and NR-fed mice for phosphorylated and total mTOR and Erk1 and ERK2.

(L) Graphical model showing that RFI drives upward of 70% of the cycling transcripts in the mouse liver.

Table S3). Many of them are involved in the regulation of carbohydrate and lipid metabolism and include, for example, cholesterol and glycogen synthesis. This therefore suggests that RFI may contribute to the temporal coordination of metabolic pathways in the mouse liver without affecting the hepatic clock.

Based on the pathways influenced by RFI, we first examined if RFI manipulation impairs circulating blood glucose level, which is circadian and at trough levels at the dark:light transition in rodents (La Fleur et al., 1999). We found that AR-fed mice exhibit an inverted rhythm in blood glucose levels when compared to NR-fed mice (Figure 4B). Since responses to boluses of insulin or glucose are also clock controlled (la Fleur et al., 2001), we performed an insulin tolerance test (ITT) at ZT2, i.e., when blood glucose levels are similar among the three groups and differences between groups cannot be confounded by differences in blood glucose levels prior to insulin injection. Surprisingly, AR-fed mice were insulin hypersensitive. 83% (10 of 12) mice displayed hypoglycemia and catatonia 90 min after insulin injection and had to be rescued by a glucose injection, whereas LB- and NR-fed mice recovered with minimal problems (Figure 4C). Because the rate-limiting enzyme for glycogen synthesis (glycogen synthase or *Gys2*) is arrhythmically expressed in AR-fed mice (Ishikawa and Shimazu, 1976; Zani et al., 2013) (Figure 3F), we examined whether the hypersensitivity to insulin in AR-fed mice may be due to abnormal reserves of glycogen, resulting in impaired restoration of circulating blood glucose levels following insulin injection. Quantification of hepatic glycogen revealed that the rhythm of glycogen levels in the liver is dampened in AR-fed mice (Figure 4D). Examination of the rhythmic expression of glycogen phosphorylase (*Pygl*), which codes for the enzyme responsible for glycogen breakdown in the liver, revealed that both catabolism and anabolism of glycogen is affected by RFI (Figures 4E and 4F). In addition, the expression of *Glut2* (aka *Slc2a2*), the main glucose transporter in hepatocytes, also shows a phase advance of 5.2 h from LB, suggesting that the availability of cellular glucose is shifted under AR feeding (Leturque et al., 2005) (Figure 4G). The expression of the glucose transporter *Glut4* (aka *Slc2a4*), which is found primarily in adipose tissues and striated muscle, is also strongly upregulated at the light:dark transition in the liver of AR-fed mice (Huang and Czech, 2007) (Figure 4G).

Considering the possibility that intracellular glucose may be repurposed through lipogenesis instead of glycogenesis, we inspected the expression of rate-limiting lipogenic enzymes (Figure 4E) and found that their expression was strongly impaired under AR feeding. While they are rhythmically transcribed with a peak at the end of the night in LB- and NR-fed mice, their expression is arrhythmic and almost out-of-phase in AR-fed mice (Figure 4H). Importantly, expression of the master lipogenic transcription factor *Srebf1* and its co-regulator, *Insig1*, is also phase advanced in AR-fed mice, suggesting that glycogenesis and lipogenesis occur simultaneously in AR-fed mice, whereas they normally occur sequentially in the liver of rhythmically fed mice (Figure 4I). Further investigation of the glycogenesis and lipogenesis pathways also revealed that paralog genes with similar rhythmic expression profiles in *ad-libitum*-fed mice exhibit a different response to RFI manipulation, i.e., only one of the two paralogs becomes arrhythmically expressed in AR-fed mice (Figures 4J and S4A). This feature, which includes genes involved in fatty acid elongation (*Elovl3* and *Elovl6*), regulation of glycogen synthesis (*Ppp1r3b* and *Ppp1r3c*), and response to insulin (*Insig1* and *Insig2*), further suggests that disruption of RFI can strongly impair the temporal organization of metabolic processes despite a functional cell-autonomous hepatic clock (Figures 4J and S4A).

To get insights into the mechanisms underlying the loss of rhythmic gene expression in AR-fed mice, we investigated the rhythmic activity of two major signaling pathways implicated in metabolism, mTOR and ERK1 and Erk2. While the total levels of mTOR and ERK1 and Erk2 proteins remains constant under all three feeding paradigms, we found that the rhythmic activation of these proteins via phosphorylation is strongly impaired in AR-fed mice (Figure 4K). Specifically, while the activity of ERK1, ERK2, and mTOR pathways are almost antiphasic in LB- and NR-fed mice, they occur coincidently throughout the 24-h day in AR-fed mice (Figure 4K). This suggests that the downstream targets of the mTOR, and ERK1 and ERK2 pathways, which include several metabolic transcription factors, may contribute to the loss of rhythmic gene expression in the livers of AR-fed mice. Taken together, our findings thus indicate that alteration in the rhythm of feeding can lead to observable changes in signaling and metabolic pathways without affecting the circadian clock (Figure 4L).

We have demonstrated that RFI drives the majority of rhythms in hepatic gene expression and contributes to the timing of signaling and metabolic pathways independently of the cell-autonomous molecular clock. It remains unknown, however, if the effects mediated by AR feeding on glucose metabolism and lipogenesis are independent of the hepatic circadian clock or if they originate from a desynchronization between clock-driven and RFI-driven rhythmic gene expression. Nevertheless, our findings that most of the rhythmic hepatic transcriptome is controlled by signals that originate from the SCN-driven rhythm of food intake rather than by the cell-autonomous hepatic clock raise the possibility that the contribution of RFI to rhythmic gene expression extends to other tissues and that other SCN-driven cues may also participate in driving peripheral rhythmic gene expression. Our data also suggest that the master circadian clock in the SCN does not act solely to synchronize peripheral circadian clocks but instead contributes more generally to circadian transcriptional programs body-wide.

Reports that liver- and other tissue-specific clock-deficient mice exhibit substantial dysregulation of rhythmic gene expression and recapitulate some of the phenotypes observed in whole-body clock-deficient mice, yet continue to eat rhythmically, indicate that clock-driven and RFI-driven transcriptional programs are likely intertwined. While the underlying mechanisms remain unclear, they may include the regulation of nutrients uptake from the portal vein or secretion of metabolites by the hepatic clock, further leading to an interdependent relationship between RFI and the cell-autonomous clock that helps maintain organismal health (Kornmann et al., 2007; Lamia et al., 2008). Finally, disruption of the clock has been shown to have far-reaching effects on aging and response to therapeutics, among others (Gorbacheva et al., 2005; Kondratov et al., 2006).

Our findings indicate that these effects could potentially be ameliorated through control of RFI, introducing an aspect of chronotherapy not yet explored.

STAR★METHODS

Detailed methods are provided in the online version of this paper and include the following:

- KEY RESOURCES TABLE
- CONTACT FOR REAGENT AND RESOURCE SHARING
- EXPERIMENTAL MODEL AND SUBJECT DETAILS
  - Animals
- METHOD DETAILS
  - Design of the feeding system
  - Manipulation of the rhythm of food intake
  - Behavioral analysis
  - RNA extraction and processing
  - Library generation and sequencing
  - Data processing
  - Rhythmicity analysis
  - Western blotting
  - Glycogen assay
  - Blood glucose assay
  - Insulin tolerance test
- QUANTIFICATION AND STATISTICAL ANALYSIS
- DATA AND SOFTWARE AVAILABILITY

SUPPLEMENTAL INFORMATION

Supplemental Information can be found online at https://doi.org/10.1016/j.celrep.2019.03.064.

ACKNOWLEDGMENTS

We thank Collin A. Osborne, Amin Heravi, Shaikh Islam, Shawn Alex, and Brooke Spann for assistance with the daily feeding of mice; Barbara Earnest for animal maintenance; Christine Merlin and Aldrin Lugena for assistance with construction of metabolic cages; Deborah Bell-Pedersen for antibodies; Heath Blackmon for bioinformatics discussion; Chaodong Wu, Honggui Li, and David Threadgill for help with physiological assays; and Allegra Fieldsend, Kate Abruzzi, and Michael Rosbash at the Brandeis Sequencing Facility for help with sequencing. This work has been supported by startup funds from Texas A&M University.

AUTHOR CONTRIBUTIONS

B.J.G. and J.S.M. conceived of and designed the experiments. All authors except E.B. contributed to the mouse-feeding experiments. J.R.B., P.F., and C.H. contributed to sample preparation. S.P., A.B., and E.B. contributed to western blot implementation and analysis. B.J.G. performed most of the bioinformatics analysis. B.J.G., A.J.T., J.R.B., and J.S.M. contributed to interpretation of results. B.J.G. and J.S.M. wrote the manuscript.

DECLARATION OF INTERESTS

The authors declare no competing interests.

Received: November 6, 2018
Revised: January 3, 2019
Accepted: March 15, 2019
Published: April 16, 2019

REFERENCES

Abbondante, S., Eckel-Mahan, K.L., Ceglia, N.J., Baldi, P., and Sassone-Corsi, P. (2016). Comparative circadian metabolomics reveal differential effects of nutritional challenge in the serum and liver. J. Biol. Chem. *291*, 2812–2828.

Albrecht, U., Zheng, B., Larkin, D., Sun, Z.S., and Lee, C.C. (2001). MPer1 and mper2 are essential for normal resetting of the circadian clock. J. Biol. Rhythms *16*, 100–104.

Atger, F., Gobet, C., Marquis, J., Martin, E., Wang, J., Weger, B., Lefebvre, G., Descombes, P., Naef, F., and Gachon, F. (2015). Circadian and feeding rhythms differentially affect rhythmic mRNA transcription and translation in mouse liver. Proc. Natl. Acad. Sci. USA *112*, E6579–E6588.

Bass, J., and Takahashi, J.S. (2010). Circadian integration of metabolism and energetics. Science *330*, 1349–1354.

Benjamini, Y., and Hochberg, Y. (1995). Controlling the false discovery rate: a practical and powerful approach to multiple testing. J. R. Stat. Soc. B *57*, 289–300.

Chaix, A., Zarrinpar, A., Miu, P., and Panda, S. (2014). Time-restricted feeding is a preventative and therapeutic intervention against diverse nutritional challenges. Cell Metab. *20*, 991–1005.

Damiola, F., Le Minh, N., Preitner, N., Kornmann, B., Fleury-Olela, F., and Schibler, U. (2000). Restricted feeding uncouples circadian oscillators in peripheral tissues from the central pacemaker in the suprachiasmatic nucleus. Genes Dev. *14*, 2950–2961.

Dobin, A., Davis, C.A., Schlesinger, F., Drenkow, J., Zaleski, C., Jha, S., Batut, P., Chaisson, M., and Gingeras, T.R. (2013). STAR: ultrafast universal RNA-seq aligner. Bioinformatics *29*, 15–21.

Doi, R., Oishi, K., and Ishida, N. (2010). CLOCK regulates circadian rhythms of hepatic glycogen synthesis through transcriptional activation of Gys2. J. Biol. Chem. *285*, 22114–22121.

Eckel-Mahan, K.L., Patel, V.R., Mohney, R.P., Vignola, K.S., Baldi, P., and Sassone-Corsi, P. (2012). Coordination of the transcriptome and metabolome by the circadian clock. Proc. Natl. Acad. Sci. USA *109*, 5541–5546.

Gorbacheva, V.Y., Kondratov, R.V., Zhang, R., Cherukuri, S., Gudkov, A.V., Takahashi, J.S., and Antoch, M.P. (2005). Circadian sensitivity to the chemotherapeutic agent cyclophosphamide depends on the functional status of the CLOCK/BMAL1 transactivation complex. Proc. Natl. Acad. Sci. USA *102*, 3407–3412.

Hatanaka, F., Matsubara, C., Myung, J., Yoritaka, T., Kamimura, N., Tsutsumi, S., Kanai, A., Suzuki, Y., Sassone-Corsi, P., Aburatani, H., et al. (2010). Genome-wide profiling of the core clock protein BMAL1 targets reveals a strict relationship with metabolism. Mol. Cell. Biol. *30*, 5636–5648.

Hatori, M., Vollmers, C., Zarrinpar, A., DiTacchio, L., Bushong, E.A., Gill, S., Leblanc, M., Chaix, A., Joens, M., Fitzpatrick, J.A., et al. (2012). Time-restricted feeding without reducing caloric intake prevents metabolic diseases in mice fed a high-fat diet. Cell Metab. *15*, 848–860.

Heinz, S., Benner, C., Spann, N., Bertolino, E., Lin, Y.C., Laslo, P., Cheng, J.X., Murre, C., Singh, H., and Glass, C.K. (2010). Simple combinations of lineage-determining transcription factors prime cis-regulatory elements required for macrophage and B cell identities. Mol. Cell *38*, 576–589.

Huang, S., and Czech, M.P. (2007). The GLUT4 glucose transporter. Cell Metab. *5*, 237–252.

Ishikawa, K., and Shimazu, T. (1976). Daily rhythms of glycogen synthetase and phosphorylase activities in rat liver: influence of food and light. Life Sci. *19*, 1873–1878.

Izumo, M., Pejchal, M., Schook, A.C., Lange, R.P., Walisser, J.A., Sato, T.R., Wang, X., Bradfield, C.A., and Takahashi, J.S. (2014). Differential effects of light and feeding on circadian organization of peripheral clocks in a forebrain Bmal1 mutant. eLife *3*, e04617.

Kaasik, K., and Lee, C.C. (2004). Reciprocal regulation of haem biosynthesis and the circadian clock in mammals. Nature *430*, 467–471.

Kawamoto, T., Noshiro, M., Furukawa, M., Honda, K.K., Nakashima, A., Ueshima, T., Usui, E., Katsura, Y., Fujimoto, K., Honma, S., et al. (2006). Effects

of fasting and re-feeding on the expression of Dec1, Per1, and other clock-related genes. J. Biochem. *140*, 401–408.

Kondratov, R.V., Kondratova, A.A., Gorbacheva, V.Y., Vykhovanets, O.V., and Antoch, M.P. (2006). Early aging and age-related pathologies in mice deficient in BMAL1, the core componentof the circadian clock. Genes Dev. *20*, 1868–1873.

Kornmann, B., Schaad, O., Bujard, H., Takahashi, J.S., and Schibler, U. (2007). System-driven and oscillator-dependent circadian transcription in mice with a conditionally active liver clock. PLoS Biol. *5*, e34.

La Fleur, S.E., Kalsbeek, A., Wortel, J., and Buijs, R.M. (1999). A suprachiasmatic nucleus generated rhythm in basal glucose concentrations. J. Neuroendocrinol. *11*, 643–652.

la Fleur, S.E., Kalsbeek, A., Wortel, J., Fekkes, M.L., and Buijs, R.M. (2001). A daily rhythm in glucose tolerance: a role for the suprachiasmatic nucleus. Diabetes *50*, 1237–1243.

Lamia, K.A., Storch, K.F., and Weitz, C.J. (2008). Physiological significance of a peripheral tissue circadian clock. Proc. Natl. Acad. Sci. USA *105*, 15172–15177.

Lawrence, M., Huber, W., Pagès, H., Aboyoun, P., Carlson, M., Gentleman, R., Morgan, M.T., and Carey, V.J. (2013). Software for computing and annotating genomic ranges. PLoS Comput. Biol. *9*, e1003118.

Leturque, A., Brot-Laroche, E., Le Gall, M., Stolarczyk, E., and Tobin, V. (2005). The role of GLUT2 in dietary sugar handling. J. Physiol. Biochem. *61*, 529–537.

Love, M.I., Huber, W., and Anders, S. (2014). Moderated estimation of fold change and dispersion for RNA-seq data with DESeq2. Genome Biol. *15*, 550.

Lück, S., Thurley, K., Thaben, P.F., and Westermark, P.O. (2014). Rhythmic degradation explains and unifies circadian transcriptome and proteome data. Cell Rep. *9*, 741–751.

Mange, F., Praz, V., Migliavacca, E., Willis, I.M., Schütz, F., and Hernandez, N.; CycliX Consortium (2017). Diurnal regulation of RNA polymerase III transcription is under the control of both the feeding-fasting response and the circadian clock. Genome Res. *27*, 973–984.

Maywood, E.S., Mrosovsky, N., Field, M.D., and Hastings, M.H. (1999). Rapid down-regulation of mammalian period genes during behavioral resetting of the circadian clock. Proc. Natl. Acad. Sci. USA *96*, 15211–15216.

Mohawk, J.A., Green, C.B., and Takahashi, J.S. (2012). Central and peripheral circadian clocks in mammals. Annu. Rev. Neurosci. *35*, 445–462.

Morgan, M., Anders, S., Lawrence, M., Aboyoun, P., Pagès, H., and Gentleman, R. (2009). ShortRead: a bioconductor package for input, quality assessment and exploration of high-throughput sequence data. Bioinformatics *25*, 2607–2608.

Panda, S. (2016). Circadian physiology of metabolism. Science *354*, 1008–1015.

Ramsey, K.M., Yoshino, J., Brace, C.S., Abrassart, D., Kobayashi, Y., Marcheva, B., Hong, H.K., Chong, J.L., Buhr, E.D., Lee, C., et al. (2009). Circadian clock feedback cycle through NAMPT-mediated NAD+ biosynthesis. Science *324*, 651–654.

Saini, C., Liani, A., Curie, T., Gos, P., Kreppel, F., Emmenegger, Y., Bonacina, L., Wolf, J.P., Poget, Y.A., Franken, P., and Schibler, U. (2013). Real-time recording of circadian liver gene expression in freely moving mice reveals the phase-setting behavior of hepatocyte clocks. Genes Dev. *27*, 1526–1536.

Satoh, Y., Kawai, H., Kudo, N., Kawashima, Y., and Mitsumoto, A. (2006). Time-restricted feeding entrains daily rhythms of energy metabolism in mice. Am. J. Physiol. Regul. Integr. Comp. Physiol. *290*, R1276–R1283.

Shearman, L.P., Zylka, M.J., Weaver, D.R., Kolakowski, L.F., Jr., and Reppert, S.M. (1997). Two period homologs: circadian expression and photic regulation in the suprachiasmatic nuclei. Neuron *19*, 1261–1269.

Stokkan, K.A., Yamazaki, S., Tei, H., Sakaki, Y., and Menaker, M. (2001). Entrainment of the circadian clock in the liver by feeding. Science *291*, 490–493.

Thaben, P.F., and Westermark, P.O. (2014). Detecting rhythms in time series with RAIN. J. Biol. Rhythms *29*, 391–400.

Thaben, P.F., and Westermark, P.O. (2016). Differential rhythmicity: detecting altered rhythmicity in biological data. Bioinformatics *32*, 2800–2808.

Trott, A.J., and Menet, J.S. (2018). Regulation of circadian clock transcriptional output by CLOCK:BMAL1. PLoS Genet. *14*, e1007156.

van der Veen, D.R., Minh, N.L., Gos, P., Arneric, M., Gerkema, M.P., and Schibler, U. (2006). Impact of behavior on central and peripheral circadian clocks in the common vole Microtus arvalis, a mammal with ultradian rhythms. Proc. Natl. Acad. Sci. USA *103*, 3393–3398.

Vollmers, C., Gill, S., DiTacchio, L., Pulivarthy, S.R., Le, H.D., and Panda, S. (2009). Time of feeding and the intrinsic circadian clock drive rhythms in hepatic gene expression. Proc. Natl. Acad. Sci. USA *106*, 21453–21458.

Wijnen, H., Naef, F., and Young, M.W. (2005). Molecular and statistical tools for circadian transcript profiling. Methods Enzymol. *393*, 341–365.

Wu, G., Anafi, R.C., Hughes, M.E., Kornacker, K., and Hogenesch, J.B. (2016). MetaCycle: an integrated R package to evaluate periodicity in large scale data. Bioinformatics *32*, 3351–3353.

Zani, F., Breasson, L., Becattini, B., Vukolic, A., Montani, J.P., Albrecht, U., Provenzani, A., Ripperger, J.A., and Solinas, G. (2013). PER2 promotes glucose storage to liver glycogen during feeding and acute fasting by inducing Gys2 PTG and G L expression. Mol. Metab. *2*, 292–305.

Zhang, P. (2012). Analysis of mouse liver glycogen content. Biol. Protoc. *2*, e186.

Zhang, R., Lahens, N.F., Ballance, H.I., Hughes, M.E., and Hogenesch, J.B. (2014). A circadian gene expression atlas in mammals: implications for biology and medicine. Proc. Natl. Acad. Sci. USA *111*, 16219–16224.

STAR★METHODS

KEY RESOURCES TABLE

REAGENT or RESOURCE	SOURCE	IDENTIFIER
Antibodies		
Rabbit anti-mTOR	Cell Signaling Technology	Cat #2972; RRID:AB_330978
Rabbit anti-phospho-mTOR Ser2448	Cell Signaling Technology	Cat #2971; RRID:AB_330970
Rabbit anti-p44/42 MAPK	Cell Signaling Technology	Cat #9102; RRID:AB_330744
Rabbit anti-phospho-p44/42 MAPK Thr202/Tyr204	Cell Signaling Technology	Cat #4376; RRID:AB_331772
Donkey anti-Rabbit IgG secondary	GE Healthcare	Cat #NA934; RRID:AB_772206
Chemicals, Peptides, and Recombinant Proteins		
TRIzol reagent	ThermoFisher	Cat #15596026
Isopropanol	EMD Millipore	Cat #PX1835-2
Ethanol	VWR	Cat #89125-176
Acid-Phenol/Chloroform, ph 4.5	ThermoFisher	Cat #AM9722
Chloroform	ThermoFisher	Cat #BP11451
Sodium acetate	ThermoFisher	Cat #AM9740
HEPES	Acros	Cat #75227-39-3
Glycerol	Sigma	Cat #G5516
EDTA	Sigma	Cat #E9884
Triton X-100	Sigma	Cat #T8787
NP-40	ThermoFisher	Cat #85124
DTT	Sigma	Cat #D9779
Phosphatase Inhibitor Cocktail	ThermoFisher	Cat #PI88266
Protease Inhibitor Cocktail	ThermoFisher	Cat #A32965
Sodium lauryl sulfate	ThermoFisher	Cat #S529-500
D-(+)-Glucose	Sigma	Cat #50-99-7
Critical Commercial Assays		
Glucose Assay Reagent	Sigma	Cat #G3293
QuantSeq 3′ mRNA-Seq Library Prep Kit	Lexogen	Cat #015.2X96
Glucometer	CVS	Cat #968574
BCA1 Kit	Sigma	Cat #B9643
QuantiFluor ssRNA	Promega	Cat #E3310
Deposited Data		
3′ mRNA-Seq Feeding Data	This paper	GEO: GSE118967
RNA-Seq *Bmal1*$^{-/-}$ Data	Atger et al., 2015	GEO: GSE73554
Raw data: Mendeley	This paper	https://doi.org/10.17632/t7gnz745kw.1
Experimental Models: Organisms/Strains		
Mouse: C57BL/6NCrl	Charles River Laboratories	Strain #027
Software and Algorithms		
ShortRead	(Morgan et al., 2009)	NA
STAR	(Dobin et al., 2013)	NA
GenomicRanges	(Lawrence et al., 2013)	NA
F24	(Wijnen et al., 2005)	NA
HarmonicRegression	(Lück et al., 2014)	NA
MetaCycle	(Wu et al., 2016)	NA
RAIN	(Thaben and Westermark, 2014)	NA
DODR	(Thaben and Westermark, 2016)	NA
HOMER	(Heinz et al., 2010)	NA

(*Continued on next page*)

Continued

REAGENT or RESOURCE	SOURCE	IDENTIFIER
Other		
Disposable Pellet Mixers and Cordless Motor	VWR	Cat #47747-358
Nitrocellulose Blotting Membrane	GE Healthcare	Cat #10600001
45mg dustless precision pellet	Bio-Serv	Cat F0165
G2 E-Mitter	Starr Life Sciences	NA
PVC Sheet	USPlastic	Cat #45095
Feeding Container	JewelrySupply	Cat #PB8301
24-hour Timer	General Electric	Cat #15119
4" PVC Tube	Home Depot	Cat #531103
4" Cap	Home Depot	Cat #39103/33463

CONTACT FOR REAGENT AND RESOURCE SHARING

Requests for further information or reagents should be directed to the Lead Contact, Jerome S. Menet (menet@bio.tamu.edu).

EXPERIMENTAL MODEL AND SUBJECT DETAILS

Animals

C57BL/6 male mice were ordered from Charles River Laboratories (ages ranging from 43 to 49 days old), and maintained in individual cages on a 12 h light:12 h dark cycle (LD12:12) with a room temperature of 22 ± 1°C. Animals were semi-randomly assigned to feeding groups such that starting body weight between all 3 feeding groups (NR, LB, AR) was not significantly different by one-way ANOVA (n = 20 mice per group). All animals were used in accordance with the guidelines set forth by the Institutional Animal Care and Use Committee of Texas A&M University (AUP #2016-0199).

METHOD DETAILS

Design of the feeding system

The feeding system we developed relies on an 8-compartment clear plastic round organizer (# PB8301, JewelrySupply) that is positioned on the top of a 24-hour timer (# 15119, General Electric), and stabilized by four screws drilled on the top of the timer and which get inserted between the organizer's compartments. The timer and food dispenser are inserted in a 4" PVC pipe (# 531103, Home Depot), and capped such that mice have access to one compartment every 3 hours (4" ABS Insert Test Cap with Knockout, #39103/33463, Home Depot). The whole system is then inserted in a standard mouse cage (N10 mouse cage, 7 1/2" x 11 1/2" x 5," #N10PLF, Ancare) drilled to accommodate the 4" PVC pipe. The entire cage/timer/pipe system is further stabilized by a custom-made support made of 1/4" gray PVC (USPlastic), and connected to electric power using an extension cord (#145-017, Home Depot).

Pilot experiments were performed to ensure that the timer was effectively doing one full rotation every 24 hours, and that mice were not hoarding food pellets. We found that putting an excess of food in each compartment (typically at the beginning of the experiment to habituate mouse to the feeding system) was associated with increased hoarding behavior, and that decreasing amounts of food to 1.5 g or less in each compartment extinguished the hoarding behavior.

Manipulation of the rhythm of food intake

Mice were fed with dustless precision pellets of 45 mg/pellet (# F0165 BioServ). Pellets are composed of 21.3% protein, 3.8% fat, 4% fibers, 8.1% ash, 54% carbohydrates, and < 10% moisture. One gram of pellet is equivalent to 3.35 kcal.

Upon arrival, mice were randomly assigned to their final feeding paradigm (*ad libitum*, arrhythmic, or night-restricted feeding), and housed individually in their cages with *ad libitum* access to food and water for one week without using the feeding system to allow them to acclimate to their new surroundings (excess of food in one compartment, timer unplugged). After one week, all mice were fed with *ad libitum* access to food using the rotating food compartments (1.5 g per compartment) to allow them to acclimate to the feeding mechanism and to calculate the daily amount of food eaten for each mouse (baseline level of food intake). After this full week under *ad libitum* feeding, we progressively adjusted the amounts of food available in each compartment for the arrhythmically-fed (AR) and night-restricted-fed (NR) mice every few days such that, after 2 weeks, all mice were on their final feeding paradigms (considered as week 0 for time of exposure to the feeding paradigm). We subjected mice to this progressive transition because sharp transition to AR- or NR-feeding paradigm results in a transitory decrease in the daily amount of food ingested per day, and a decrease in body weight. For all experiments, *ad libitum* (LB) mice had an excess of food placed within each compartment of the container (1.5 g), such that they never lacked for food. AR-fed mice had their daily food intake split evenly among the

8 compartments. NR-fed mice had their daily food split evenly among the 4 compartments corresponding to the night. All mice had *ad libitum* access to water.

Food containers were changed every day at ZT8 (3pm). Records of food placed within each compartment for each mouse, as well as food remaining after retrieving the container, were made to keep track of how much each mouse ate every 3 hours. Every 2 days, the total amount of food eaten by each mouse was assessed and potentially increased or decreased in order to maintain mice on their feeding paradigms. For example, mice on controlled feeding (AR or NR) that ate all pellets for two consecutive days were given two more pellets in opposite compartments such that their daily profile of food eaten did not change in rhythmicity. Similarly, mice that consistently had 4 or more pellets remaining for two consecutive days were given two less pellets, one each in opposite compartments. The intent was to end each day with 1-2 pellets remaining in total for each mouse, indicating that the mouse was calorically satisfied without either a suspicion of starvation or an excess of food available.

Behavioral analysis

Mice aged 43-49 days were implanted with a sterile G2 E-Mitter (Starr Life Sciences) into the peritoneal cavity while anesthetized under a steady flow of 2% isoflurane in 100% O_2. Slow release Buprenorphine (1mg/kg) was injected interperitoneally beforehand for pain relief. Mice were allowed to recover for 2 weeks before testing of the data collection system. Final data shown in the manuscript were collected for 1 week 3 months post-surgery. Data were collected over 10-minute intervals and binned into 30 minute intervals for analysis. Data collected during the first hour of recording was discarded to avoid bias from system initialization.

RNA extraction and processing

After 5 weeks of exposure to AR-, LB-, or NR-feeding paradigm, mice were anesthetized with isoflurane, decapitated, and the liver collected. The left lateral lobe was cut into three equivalent-sized pieces for RNA processing, with the remainder of the liver stored together. All collected tissues were flash-frozen in liquid nitrogen and stored at −80°C. One third of the left lateral lobe of the liver was used for RNA extraction and purification. RNA was extracted from frozen tissue using TRIzol and following manufacturer's recommendations. Briefly, the frozen tissue was mixed with 300μL of TRIzol reagent, homogenized using a pellet mixer, and the volume brought to 1mL with 700μL of TRIzol reagent. 200μL chloroform was added, and the solution shaken and centrifuged at 12,000 g for 15 minutes at 4°C. The aqueous phase was extracted and added to an equivalent amount of isopropanol. The resulting solution was that centrifuged at 12,000 g for 10 minutes at 4°C, and the RNA pellet was washed with 1mL of 75% ethanol before being resuspended with 25μL RNase-free deionized water. Total RNA was then purified with an acid phenol/chloroform extraction, and precipitated by ethanol precipitation. The RNA pellet was then washed with 75% ethanol as described above, and finally resuspended in 25μL. Samples were quantified with a NanoDrop-1000 and with the Promega QuantiFluor ssRNA system, and quality / integrity of total RNA was assessed by gel electrophoresis.

Library generation and sequencing

RNA-Seq libraries were generated using the Lexogen QuantSeq 3′mRNA-Seq Library Prep Kit following manufacturer instructions, with 2 μg of total RNA used as starting material. cDNA was PCR-amplified for 12 cycles following manufacturer recommendations for mouse liver tissue. Libraries were multiplexed in equimolar concentrations and sequenced in two runs using an Illumina NextSeq 500 platform (Brandeis University, USA).

Data processing

Sequenced reads were pre-processed with the R package ShortRead (Morgan et al., 2009) to remove the first 12nt, remove low-quality bases at the 3′ end, trim poly-A tails and embedded poly-A sequences, and remove all reads under 36nt in length. Reads were aligned to the mm10 transcriptome, assembly GRCm38.p4, with the STAR aligner(Dobin et al., 2013) version 2.5.2b with options–outSAMstrandField intronMotif–quantMode GeneCounts–outFilterIntronMotifs RemoveNoncanonical. Secondary alignments were removed with samtools view -F 0x100. Read counts were summarized with the function countOverlaps from the R package GenomicRanges (Lawrence et al., 2013) and normalized by library size to a total of 1 million reads per library, resulting in a matrix of transcripts per million (TPM). Normalization to gene size was not performed, as we performed 3′-mRNA sequencing. Finally, only genes with greater than 1TPM in at least 36 of the 72 samples were kept to form the final count matrix with 11536 genes.

To ensure quantification of the same transcriptome annotations between our dataset and that of Atger et al., 2015, RNASeq data were downloaded from GEO, accession ID GSE73552. Reads were mapped to the mm10 transcriptome, assembly GRCm38.p4, using the STAR aligner version 2.5.2b with options–outSAMstrandField intronMotif–quantMode GeneCounts–outFilterIntronMotifs RemoveNoncanonical–outSAMtype BAM SortedByCoordinate–seedSearchStartLmax 15–clip3pAdapterSeq TGGAATTCTCGGGTGCCAAGGAACTCCAGTCAC–outReadsUnmapped Fastx, to replicate the original mapping procedure. Secondary alignments were removed with samtools view -F 0x100. Read counts were summarized with countOverlaps from GenomicRanges and normalized to FPKM values using DESeq2 (Love et al., 2014).

Rhythmicity analysis

Rhythmic analysis of the three major feeding paradigms (NR, LB, and AR) was performed with four programs: F24 (Wijnen et al., 2005), MetaCycle (Wu et al., 2016), HarmonicRegression (Lück et al., 2014), and RAIN (Thaben and Westermark, 2014). DR was

not included in rhythmic analysis or used to form categories, but is shown in Figure 2C to examine the effects of a feeding rhythm intermediate between LB and AR on rhythmic gene expression. Program-specific settings were as follows:

F24: iterations = 10000
MetaCycle: adjustPhase = 'predictedPer', combinePvalue = 'fisher'
HarmonicRegression: normalize = FALSE
RAIN: period = 24, deltat = 4, nr.series = 3, peak.border = c(0.2, 0.8), method = 'independent'

Resulting p values were adjusted using the Benjamini-Hochberg method within the p.adjust function available in base R (Benjamini and Hochberg, 1995) to control for the false-discovery rate (FDR). Genes that were found to be rhythmic (BH-adjusted p value –aka q-value– $\leq$ 0.05) in at least 2 of the 4 rhythmic programs per feeding paradigm were considered as rhythmic for that feeding paradigm (Table S1). The rhythmic amplitude (rAMP) as reported by MetaCycle was taken for all genes within each category and feeding paradigm.

Western blotting

Frozen liver tissue was incubated in 300 μL of ice-cold RBS buffer (20mM HEPES, 50mM KCl, 10% glycerol, 2mM EDTA, 1% Triton X-100, 0.4% NP-40, 1X phosphatase inhibitor cocktail, 1mM DTT, and 1X Protease inhibitor cocktail) and homogenized on ice. Homogenate was centrifuged at 4°C for 10 minutes at high speed and the supernatant extracted. Protein abundance was quantified with the BCA1 kit (Sigma-Aldrich #B9643) following manufacturer instructions. Samples were run on SDS-PAGE gels and semi-dry transferred to a nitrocellulose membrane. Antibody information can be found in the STAR Methods section. All of them were used at a concentration of 1:1000.

Glycogen assay

Hepatic glycogen was quantified through a method modified from Zhang et al., 2014 (Zhang, 2012). In brief, measured amounts of crushed frozen tissue were placed into tubes containing 500 μL of 2M HCl (sample) or 2M NaOH (control) and heated on a hot block set to 95°C for one hour, shaken at 10 minute intervals. An equivalent amount of 2M NaOH (for samples) or 2M HCl (for controls) was added to neutralize the acidic and basic conditions, followed by centrifugation at 20000 g for 10 minutes. 10 μL was used for quantification with the Glucose Assay Reagent, following manufacturer specifications, with a 0.5mM solution of dextrose used as a standard. Total glycogen was quantified by subtracting the signal of the undigested control from the digested sample and normalizing to the standard signal and tissue weight. Each batch (1 rhythm of each feeding paradigm) was normalized such that the total signal was equivalent between batches.

Blood glucose assay

0.5 mm of the tail tip of each mouse was removed and blood collected in a 25 μL capillary until approximately half full. Each time point was spaced 3 days apart to avoid causing anemia from blood loss. Collected blood was expelled into a sodium heparin-coated microfuge tube, sealed, and shaken in order to coat the blood with heparin and prevent congealing. Samples were centrifuged at 10000 g for 5 minutes and blood plasma collected from the upper layer. Plasma glucose was measured using a glucometer (CVS Health #968574). The lowest value that the glucometer could report was 20mg/dL (anything under this was reported as 'Low'), and so samples under this threshold were recorded as 20.

Insulin tolerance test

Food containers and water bottles were removed from each cage at ZT22, i.e., 4 hours before insulin injection. 5IU/kg body weight of insulin (Novalin R) was injected at ZT2. Blood was collected from the tail tip of each mouse just prior to injection and every 30 minutes afterward for 2 hours, and glucose measured as described for the blood glucose assay. 83% (10 of 12) of AR-fed mice were catatonic and unresponsive at the 90-minute collection time (responsiveness determined by testing the toe pinch reflex), and were rescued after blood collection at that time with an injection of 20% glucose at 0.1mL/10 g mouse. As a result, blood from AR-fed mice was not collected at the 120-minute mark.

QUANTIFICATION AND STATISTICAL ANALYSIS

Statistical analyses were performed using core R functions. Plots of feeding-related gene expression (Figures 3A, 3E, 3F, 4F–4J, and S3A) are displayed as mean TPM ± s.e.m, n = 3 mice per time point and feeding paradigm. Plots of gene expression profiles originating from the Atger et al., 2015 datasets (Figures 3E, 3F, S3A, and S4A) are displayed as mean FPKM ± s.e.m., n = 4 mice per time point for wild-type mice and n = 2 mice per time point for *Bmal1*$^{-/-}$ mice. Differences between groups (n = 18) in Figure 1C were analyzed with a repeated-measures two-way ANOVA, with Before|After and Day|Night as factors. # denotes a significant interaction (p value < 0.05). Quantification of physiological data (Figures 1D–1F) was performed by binning data into 30 minute intervals and is represented as mean ± s.e.m. with n = 7-8 mice per feeding paradigm. Differences between the three physiological

measurements were determined through pairwise t tests between matching measurements (*e.g.*, the body temperature during the day in NR-fed mice was only compared to the body temperature during the day in AR- and LB-fed mice).

Comparisons of rhythmic amplitude between feeding paradigms and rhythmic categories (Figure 2B) was performed by taking the relative amplitude (rAMP) reported by MetaCycle (Wu et al., 2016) for all genes within each of the four categories, and sorted by feeding paradigm. Differences in rAMP between groups were determined by a Kruskal-Wallis test within each rhythmic category followed by a post hoc Wilcoxon pairwise test with the Bonferroni correction.

Differential rhythmicity, detected as changes in peak phase and/or rhythmic amplitude, was tested within the two different datasets using DODR (Thaben and Westermark, 2016). In the rhythmic feeding dataset, AR was tested against NR. In the dataset from Atger et al., 2015, wild-type was tested against *Bmal1*$^{-/-}$. In both cases, genes were considered significant if the p value of the resulting HANOVA test was less than or equal to 0.05. Differences in response to AR versus NR and WT versus *Bmal1*$^{-/-}$ between rhythmic categories were compared with pairwise Kolmogorov-Smirnov tests and are plotted as the $\log_{10}$-transformed p values versus the cumulative distribution of p values within each group (Figure 3D).

Comparisons between the feeding dataset and the dataset from Atger et al., 2015 (Figures 3C and S3B) were performed by binning all genes within the RRR, RRA, RAA, and AAR categories by phase into 6 bins representing 4 hours each, starting with ZT0. Expression data for each gene within both datasets was standardized to z-scores, and plotted as the median within each bin ± 95% confidence interval.

Blood glucose levels (Figure 4B) and insulin tolerance blood glucose levels (Figure 4C) were tested with a repeated-measures two-way ANOVA (Paradigm × Time point). Individual time points are analyzed with a one-way ANOVA on paradigms. Hepatic glycogen (Figure 4D) was analyzed for overall differences with a two-way ANOVA (Paradigm × Time point), with individual time points analyzed with a one-way ANOVA on paradigms.

DATA AND SOFTWARE AVAILABILITY

The RNA-Seq datasets generated in this paper are available at Gene Expression Omnibus (GEO) under the accession number GEO: GSE118967. Raw data for the western blot analysis are freely accessible via the following link: https://doi.org/10.17632/t7gnz745kw.1 (Mendeley).

Cell Reports, Volume *27*

Supplemental Information

Rhythmic Food Intake Drives Rhythmic Gene Expression More Potently than the Hepatic Circadian Clock in Mice

Ben J. Greenwell, Alexandra J. Trott, Joshua R. Beytebiere, Shanny Pao, Alexander Bosley, Erin Beach, Patrick Finegan, Christopher Hernandez, and Jerome S. Menet

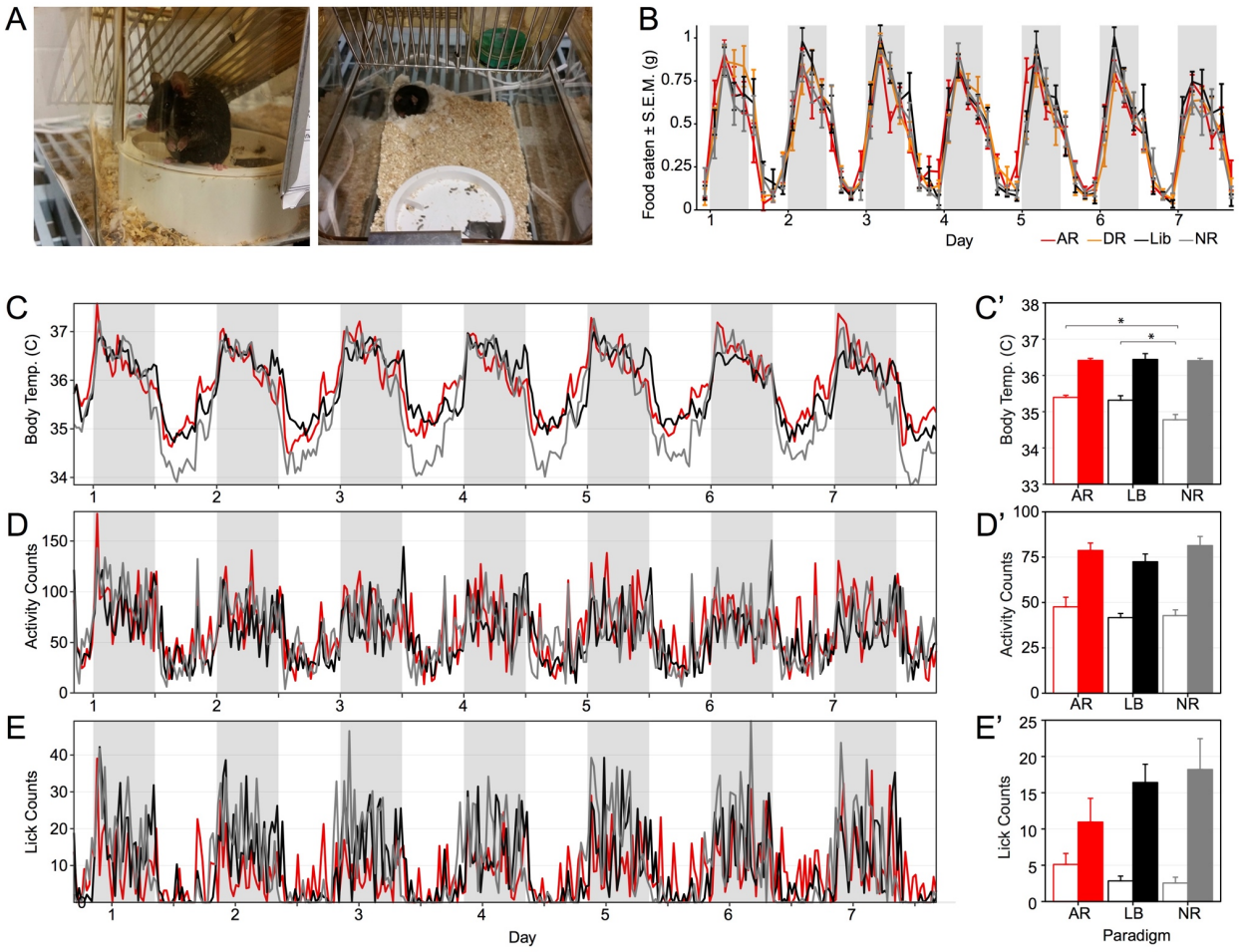

Figure S1: Mice fed arrhythmically remain behaviorally rhythmic (related to Figure 1). **(A)** Pictures of the feeding system. Note that the lid blocks the access to 7 out of the 8 food compartments such that only 3 hours of food is available at one time. **(B)** Food eaten from each of the eight compartments for the first seven consecutive days of feeding while mice are all on *ad libitum* feeding, n=18 per feeding paradigm. AR: arrhythmic feeding (red); DR: dampened feeding rhythm (orange); LB: *ad libitum* feeding (black); NR: night-restricted feeding (gray) **(C-E)** Seven consecutive days of body temperature, physical activity, and lick counts that are averaged in Figure 1D-F (n=7-8 per feeding paradigm). (C'-E') Quantification of the seven consecutive days represented in (C-E), with empty bars corresponding to the data recorded during daytime, and solid bars to data recorded during nighttime.

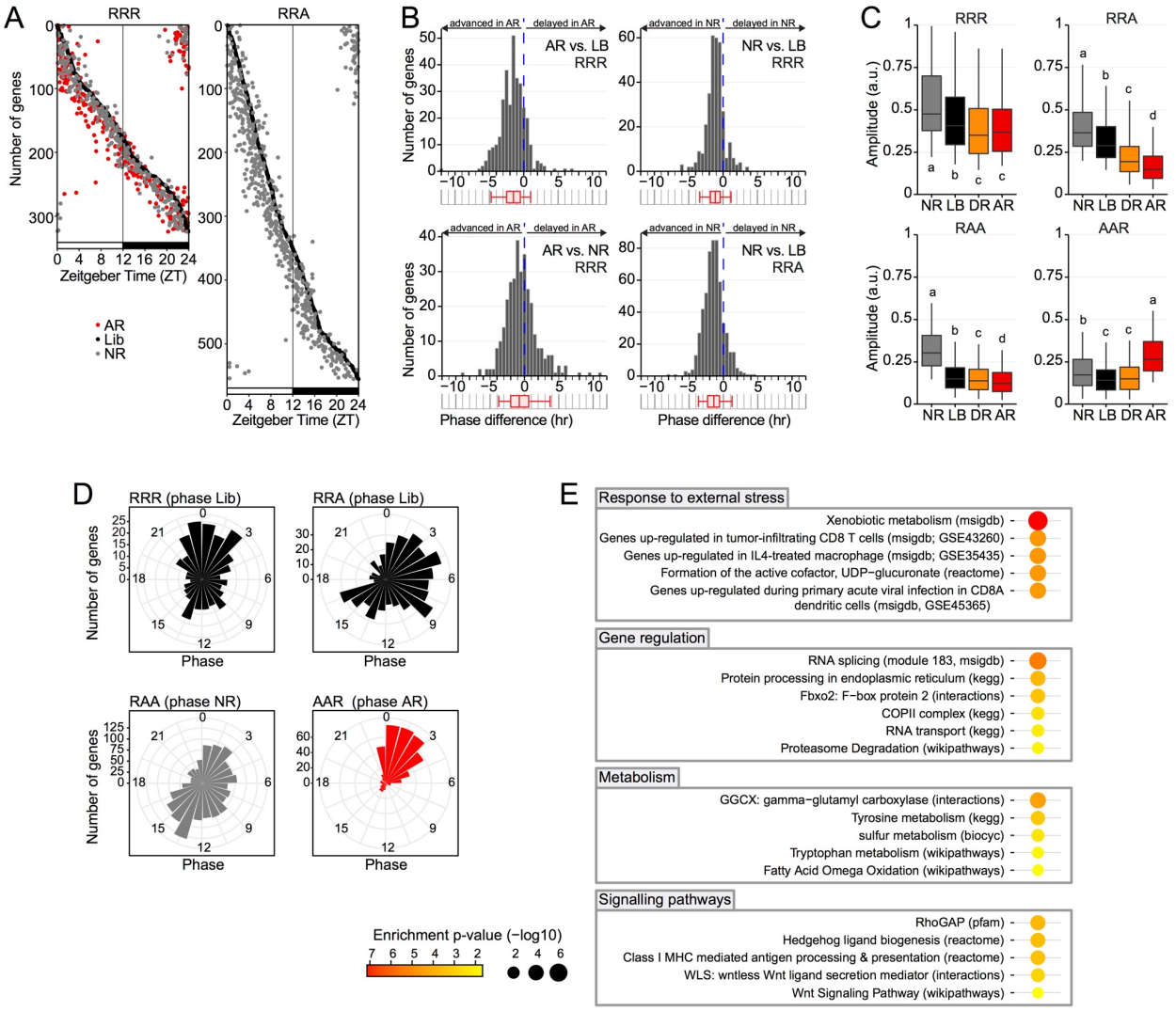

Figure S2: Manipulation of rhythmic food intake impairs rhythmic gene expression in the mouse liver (related to Figure 2).
(A) Phase of the 324 and 555 rhythmic genes within the RRR (genes rhythmic in NR-, LB-, and AR-fed mice) and RRA (genes rhythmic in NR- and LB-fed mice, and arrhythmic in AR-fed mice) categories for each feeding paradigm, respectively, organized by increasing phase in LB. **(B)** Phase difference of rhythmic expression between NR-, LB-, and AR-fed mice for the 324 and 555 rhythmic genes within the RRR and RRA categories, respectively. **(C)** Relative amplitude (rAMP) as reported by MetaCycle for all genes within each of the four categories, and sorted by feeding paradigm. **(D)** Rose plots of the phase of rhythmic genes within each category. Phases are taken such that LB is used whenever possible; otherwise, the phase from the most rhythmic feeding paradigm expressed in that category is used. Categories shown are RRR (genes rhythmic in NR-, LB-, and AR-fed mice; 324 genes), RRA (genes rhythmic in NR- and LB-fed mice, and arrhythmic in AR-fed mice; 555 genes), RAA (genes rhythmic in NR-fed mice only; 1674 genes), and AAR (genes rhythmic in AR-fed mice only; 495 genes). **(E)** Pathway enrichment for the AAR genes.

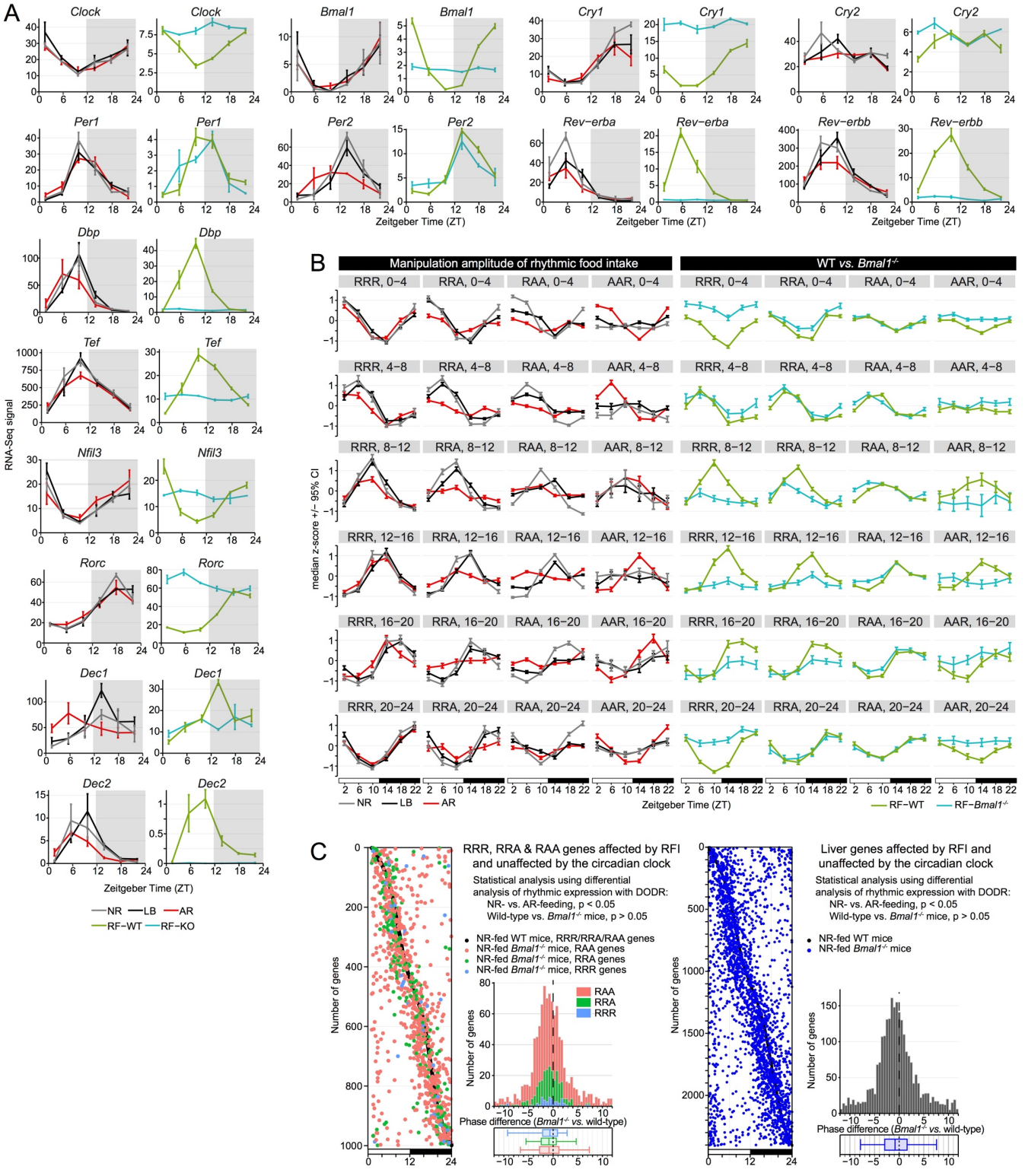

Figure S3: Rhythmic food intake drives most hepatic rhythmic gene expression independently of the hepatic clock (related to Figure 3).

(A) Clock gene mRNA expression in the mouse liver. Left: expression in the liver of mice fed arrhythmically (AR; red), *ad libitum* (LB; black), and only at night (NR; gray); datasets from this

study. Right: expression in the liver of wild-type and *Bmal1*$^{-/-}$ mice fed only at night; dataset from Atger et al., 2015. **(B)** Genes within the RRR, RRA, RAA, and AAR categories (see description below) were binned by phase into 4-hour groups and their expression in both the RFI manipulation datasets and *Bmal1*$^{-/-}$ datasets (from Atger et al. 2015) were standardized separately. The standardized median value ± 95% confidence interval for each timepoint, binned group, and rhythmic category were then plotted for both datasets. RRR (genes rhythmic in NR-, LB-, and AR-fed mice; 324 genes), RRA (genes rhythmic in NR- and LB-fed mice, and arrhythmic in AR-fed mice; 555 genes), RAA (genes rhythmic in NR-fed mice only; 1674 genes), and AAR (genes rhythmic in AR-fed mice only; 495 genes). **(C)** Phase distribution and phase difference between wild-type vs. *Bmal1*$^{-/-}$ mice for genes significantly affected by rhythmic food intake (NR-fed *vs*. AR-fed gene expression; DODR p-value ≤ 0.05) but not affected by circadian clock disruption (wild-type *vs*. *Bmal1*$^{-/-}$ mice; DODR p-value > 0.05). Left: analysis on genes from the RRR, RRA, and RAA categories. Right: analysis on all genes expressed in the mouse liver. Mouse liver gene expression in wild-type and *Bmal1*$^{-/-}$ mice were retrieved from a public dataset (Atger et al. 2015).

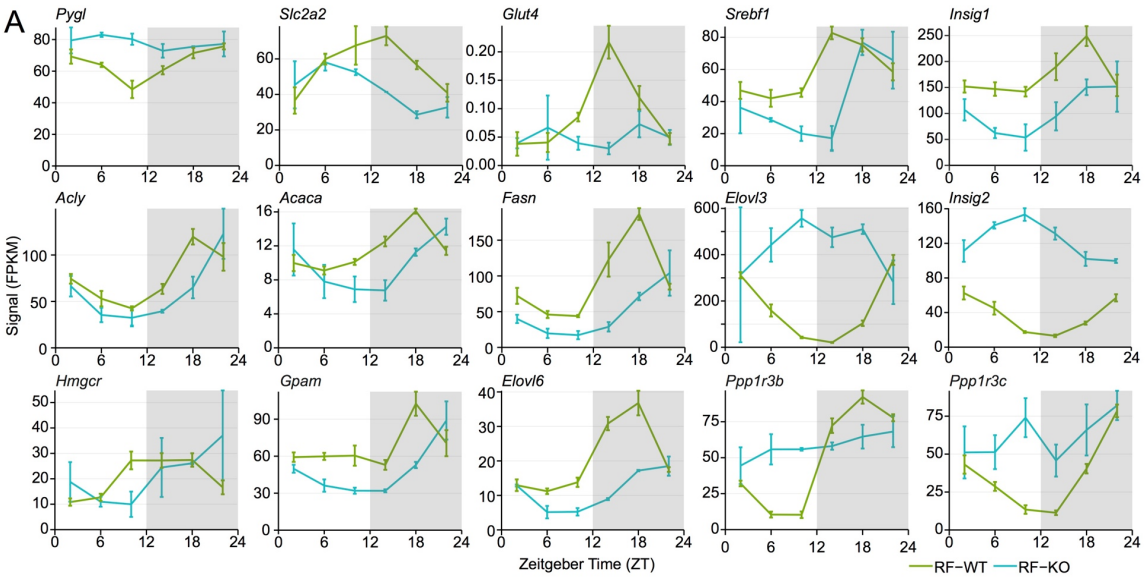

Figure S4: Rhythmic food intake contributes to the timing of metabolic and signaling pathways independently of the hepatic clock (related to Figure 4).
(A) Mouse liver mRNA expression for genes involved in glycogenesis, lipogenesis, and cholesterol biosynthesis in wild-type (green) and *Bmal1*$^{-/-}$ (cyan) mice fed only at night (datasets from Atger, et al. 2015). Effect of RFI manipulation on the expression of these 15 genes in the mouse liver is shown in Figure 4F-J.

Table S1 (related to STAR Methods): Statistical analysis of rhythmic gene expression.

Table S1A: Number of rhythmically expressed genes in the mouse liver based on the feeding paradigm and the statistical program (q-value≤ 0.05). AR: arrhythmic feeding; LB: *ad libitum* feeding; NR: night-restricted feeding.

Program	AR	LB	NR
Harmonic regression	390	800	1814
Metacycle	1345	1630	3103
F24	417	880	1874
RAIN	1527	2287	3344

Table S1B: Number of rhythmically expressed genes based on the feeding paradigm (AR: arrhythmic feeding; LB: *ad libitum* feeding; NR: night-restricted feeding) and the number of programs that classify a gene as rhythmically expressed (q-value≤ 0.05). The four programs used were Harmonic regression (Luck et al., 2014), Metacycle (Wu et al., 2016), F24 (Wijnen et al., 2005), and RAIN (Thaben and Westermark, 2014).

Number of programs	AR	LB	NR
1	1811	2473	3767
2	1061	1454	2718
3	448	912	1926
4	359	758	1724